ChemComm



COMMUNICATION

View Article Online



Cite this: *Chem. Commun.*, 2023, **59**, 9525

Received 24th April 2023, Accepted 4th July 2023

DOI: 10.1039/d3cc01996a

rsc li/chemcomm

Strong metal-support bonding enhanced thermal stability in Au-Al₂O₃ core-shell nanowires characterized by *in situ* transmission electron microscopy†

Haotian Yang, ¹D^a Claron J. Ridge, ^b Kyle Overdeep, ^b C. Michael Lindsay, ^b Xiao Tong ¹D^c and Alexander Orlov*^a

In this study, the thermal stability of $Au-Al_2O_3$ core-shell and Au nanowires was investigated by *in situ* scanning transmission electron microscopy and other techniques. The nanowires were synthesized by the helium droplets method and deposited on various substrates. The *in situ* characterization of $Au-Al_2O_3$ thermal stability demonstrated a substantially enhanced stability as compared to that of pure Au nanowires, which can be a transformative approach to design more durable Au-based nanocatalysts. Our study also revealed the existence of strong metal-support bonding in the Au/Al_2O_3 system.

In recent decades, a large number of studies have been focused on nano-structured Au catalysts given their improved surface area, as well size-tunable and morphology-dependent properties. Importantly, these nanostructured materials are promising candidates for the next generation of catalysts for such essential catalytic reactions as CO oxidation and CO2 reduction. Despite their high catalytic activity, Au nanocatalysts tend to agglomerate at high temperature and become inactive, which is especially noticeable for size-sensitive reactions.² As a result, their applications for industrial catalysis are rather limited. It is well known that interaction between metal nanoparticles (NPs) and supporting metal oxides plays a key role in determining the stability and lifetime of catalysts.³⁻⁶ The strength of the metalsupport bonding (MSB) is a critical factor to determine the stability⁷ and catalytic activity⁸ of catalysts. For example, Al₂O₃ is often used as a support for Au nanoparticles, where MSB between Au and Al₂O₃ results in high catalytic stability.^{9,10} It was shown that in these catalytic systems, Au particle size

remained within the 2 ± 0.8 nm range even after calcination at 700 °C. However, fundamental studies focused on developing a better understanding of the enhanced thermal stability of such supported systems using *in situ* methods are still lacking, which hinder designing of the next generation of nanocatalysts.

In addition to stability, there are also synthetic challenges in designing these catalytic systems, as conventional synthetic methods always utilize organic capping agents that can obstruct surface catalytic reactions and affect thermal stability of catalysts. 11 In contrast to traditional synthetic methods, 4 He (HeII) is an outstanding templating medium to form nanostructures, given its distinct properties. Firstly, due to weak interactions between He atoms, helium clusters still remain liquid at temperatures that are very close to 0 K. 12 Secondly, it is superfluid at temperature below 2.172 K and exhibits exceptionally high thermal conductivity. It also has the ability to capture metallic vapor to form catalytically active single phase and core-shell NPs,1 which can be achieved by either one-step or a sequential evaporative process. 13 Moreover, given the strong pressure gradients and one-dimensional structure to attract atoms, quantized vortices in superfluid helium can force metal atoms to form 1D metallic nanowires with high surfacevolume ratio to promote catalytic reactions, 14-18 which are otherwise challenging to produce using the conventional templating methods. Finally, given the soft landing nature of liquid helium droplets, 13 the nanostructures inside the droplets can cushion the landing of nanoparticles and preserve their shape.

In this work, the evidence of strong metal–support bonding (SMSB) between Au and Al_2O_3 shell in $Au-Al_2O_3$ core–shell nanowires (NWs) was demonstrated by a combination of *in situ* scanning transmission electron microscopy (STEM), energy dispersive X-ray spectroscopy (EDS) and X-ray photoelectron spectroscopy (XPS) experiments. Given the nature of He nanodroplet deposition, it was possible to synthesize pure $Au-Al_2O_3$ core–shell and Au nanowires that avoided surface contamination that is typical in other methods of synthesis. Moreover, by employing a multi-slot substrate holder that was

^a Department of Materials Science and Chemical Engineering, Stony Brook University, Stony Brook, New York 11794, USA. E-mail: alexander.orlov@stonybrook.edu

^b Energetic Materials Branch, US Air Force Research Laboratory, Eglin Air Force Base, Florida 32542, USA

^c Center for Functional Nanomaterials, Brookhaven National Laboratory, Upton, New York 11793 USA

[†] Electronic supplementary information (ESI) available. See DOI: https://doi.org/10.1039/d3cc01996a

subjected to highly repeatable deposition conditions, it was possible to synthesize the nanowires with identical morphology and chemical composition. A notable highlight of our results is that Au-Al₂O₃ core-shell NWs remained cylindrical during in situ heating at 500 °C for 30 minutes, while morphology of pure Au nanowires changed from cylindrical to spherical within the same temperature and time range. This enhanced thermal stability of Au-Al₂O₃ NWs indicated the existence of SMSB in Au/Al₂O₃ system that preserved its shape. To the best of our knowledge, this is the very first demonstration of SMSB in Au- Al_2O_3 system using in situ experiments. Importantly, this new

Communication

More specifically, the bimetallic nanowires were synthesized by He nanodroplets deposition method and deposited on both Si₃N₄ TEM grids and Si₃N₄ coated Si wafer in inert conditions for subsequent TEM/STEM and XPS characterization. The details of characterization techniques can be found in ESI.†

approach can be extended to other gold/metal oxide systems.

Fig. 1 shows the sequence of helium nanodroplets deposition to produce Au-Al₂O₃ core-shell NWs. First, He gas was cooled to 4.5 K by passing it through a nozzle, which created He nanodroplets. Next, the vaporized Al and Au atoms were captured by nanodroplets beam. The subsequent Al and Au condensation inside the droplets, which was driven by a quantized vortices phenomenon,15 resulted in formation of bimetallic NWs. Finally, the flying NWs were captured on both Si₃N₄ substrates and TEM grids using soft landing conditions. The detailed deposition parameters can be found in ESI.†

The morphology of Au NWs and Au-Al₂O₃ core-shell NWs is illustrated in Fig. 2. The coexistence of both Au-Al₂O₃ and Au NWs on substrate was a result of nonuniform capture of Au and Al vapor, since not all of the nanodroplets could capture both Au and Al atoms during the deposition. The length of NWs varied from 10 nm to more than 100 nm. The core-shell structure of NWs can be clearly seen in Fig. 2b, where darker colours are indicative of Au lattice pattern located in the center of NWs, which was surrounded by a more transparent Al₂O₃ shell. Despite the fact that nanodroplets flew first through evaporated Al atoms cloud followed by Au cloud, Au atoms formed a core of NWs instead of a shell. There are two possible reasons to explain this phenomenon: firstly, in binary alloys, the diffusivity of Al is much higher than that of Au in liquid phase; 19 secondly, the surface tension of Al is lower than that of Au.²⁰ Therefore, when the He droplets trapped both Au and Al

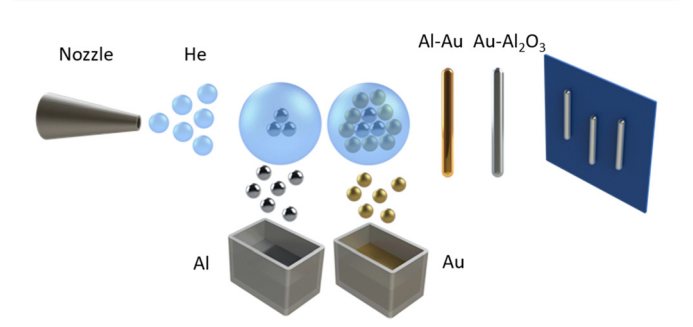
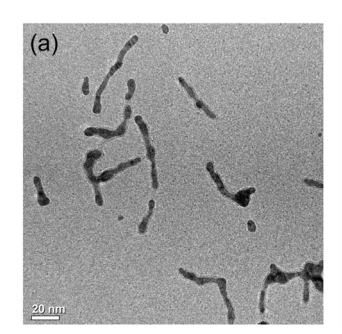


Fig. 1 Schematic of helium nanodroplet deposition method to deposit Au-Al₂O₃ nanowires.



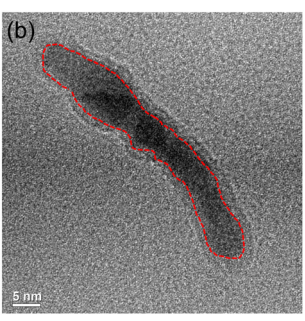


Fig. 2 TEM images of pure Au and Au-Al₂O₃ nanowires. (a) Overview of pure Au and Au-Al₂O₃ nanowires. (b) Higher magnification TEM image of single Au-Al₂O₃ core-shell nanowire. Au core is highlighted by red line.

atoms, Al atoms diffused towards Au surface to lower the surface energy, thereby forming a more thermodynamically stable system. Following the deposition and subsequent exposure to air, Al was oxidized to Al₂O₃ to form Au-Al₂O₃ core-shell NWs. EDS maps and line scan of the cross-section of Au-Al2O3 NWs clearly showed the core-shell structure (Fig. S1 and S2, ESI†).

In situ STEM characterization of Au-Al2O3 core-shell and pure Au NWs before and after heating is shown in Fig. 3. The nanowires were heated under high vacuum from room temperature to 500 °C using 100 °C min⁻¹ heating rate. Following heating for 15 minutes (Fig. 3b), most of the nanowires shrank to particles and their morphology remained unchanged during the 30 minutes of subsequent heating (Fig. 3c). However, a few nanowires (highlighted by blue circles) had maintained their cylindrical shape throughout the heating cycle with some minor reduction in their lengths. This phenomenon is consistent with previous studies where Au nanowire thermal instability was observed even at temperatures below 100 °C.21 On the other hand, it is conceivable that Al₂O₃ shell improved the thermal stability of Au nanowires that stayed cylindrical during the heating.

To verify our hypothesis, in situ EDS experiment was conducted on Au-Al2O3 and pure Au NWs to reveal the heat induced evolution in elemental distribution of Au and Al. The heating rate replicated the one in STEM experiment. After 30 minute of heating the sample was cooled to RT prior to EDS imaging. The core-shell structure of Au-Al₂O₃ NWs before heating is shown in Fig. 4a-d. Based on the combined Au/Al (Fig. 4d), and individual Au (Fig. 4c) and Al (Fig. 4b) EDS mapping, we confirmed that Au NWs were encapsulated in Al₂O₃ shell. The reason for the Al shell not being adequately resolved in the HAADF image (Fig. 4a), as compared to that in EDS mapping (Fig. 4d), is due to a large difference in the atomic numbers of Al (13) and Au (79) that correlates to the pixel brightness. More specifically, the brightness is proportional to the square of elements' atomic number (Z^2) . As a result, the intensity of Au related pixels was about 37 times higher than that of Al for the samples of the same thickness. Therefore, the signal coming from the Al shell was overwhelmed by a signal coming from Au (Fig. 4a). After heating, the length of nanowire slightly decreased from 25.4 nm to 20.5 nm and remained cylindrical shape with the core-shell structure unchanged. This

ChemComm Communication

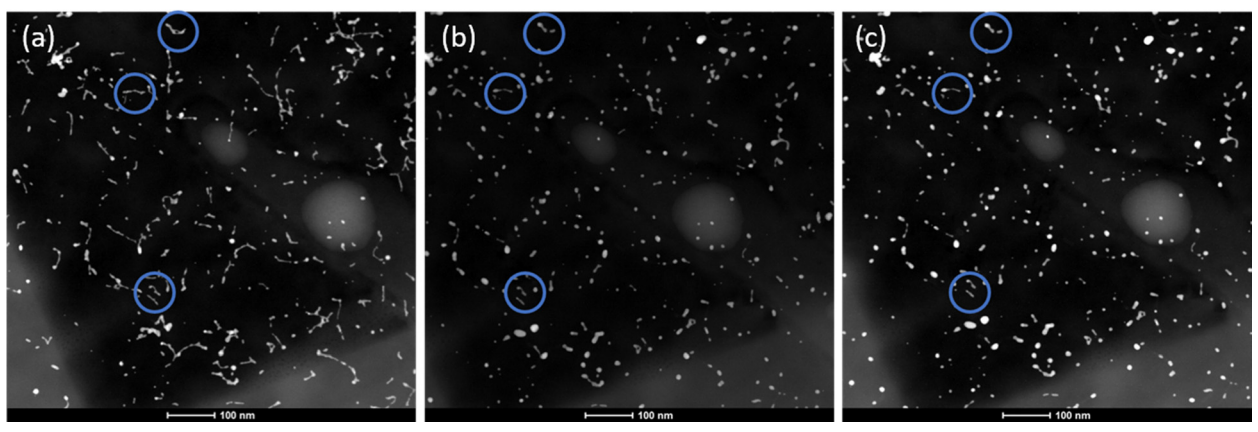


Fig. 3 Morphology evolution of Au-Al₂O₃ core-shell, and pure Au NWs in RT (a), heated for 15 minutes (b) and 30 minutes (c) at 500 °C. Scale bar:

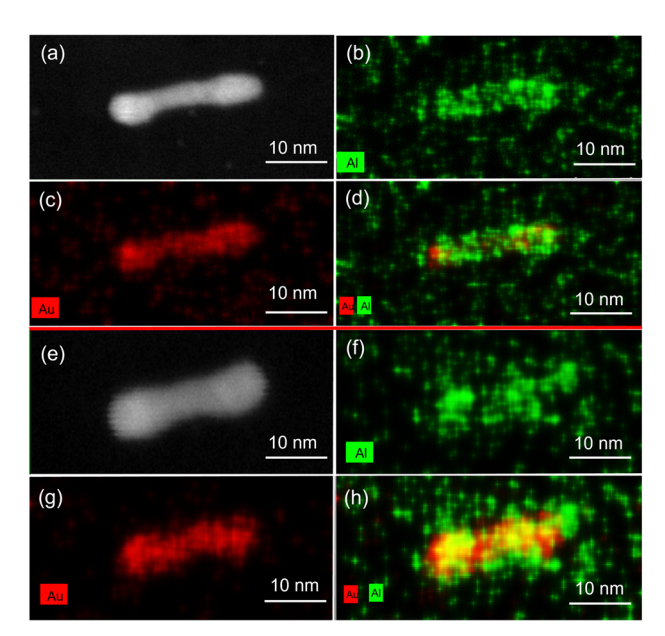


Fig. 4 HAADF STEM image and EDS maps of single Au-Al₂O₃ nanowire before (a-d) and after heating (e-h). (a) and (e) HADDF STEM images. (b), (f) and (c), (g) Al and Au EDS maps. (d) and (h) Combined Al and Au EDS maps. Scale bar: 10 nm.

confirmed a stabilizing effect of Al₂O₃ shell on Au NWs. Extended heating experiment of exploring the breakpoint of the core-shell structure will be conducted in the future.

To benchmark the above-mentioned results, a pure Au NW is shown in Fig. 5, where only Au signal could be observed while Al₂O₃ shell was not detected either before (Fig. 5b) or after heating (Fig. 5f). In the absence of the protective Al₂O₃ shell, the nanowire shrank to a spherical nanoparticle (Fig. 5e and g). More specifically, following the heating, the NW length reduced from 32.4 nm to 13.9 nm.

It is important to mention that there is a gap in literature on mechanistic aspects of improved stability of Au nanowires stabilized by Al₂O₃. However, there are studies confirming thermal stability of Au nanoparticles protected by oxide

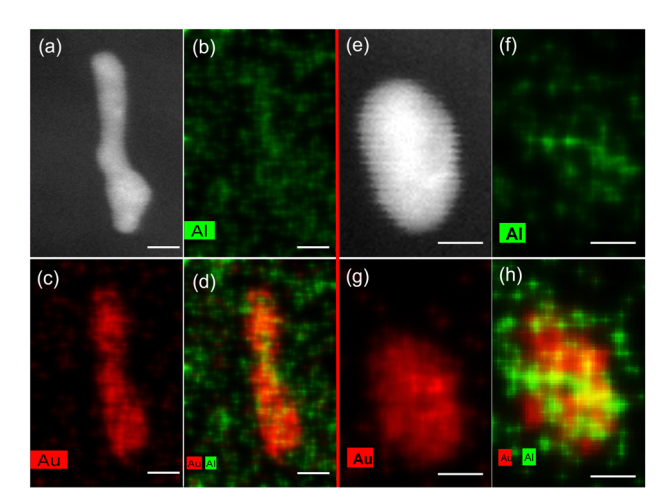


Fig. 5 HAADF STEM image and EDS maps of Au nanowire before (a-d) and after heating (e-h). (a) and (e): HADDF STEM images. (b), (f) and (c), (g): Al and Au EDS maps. (d) and (h): combined Al and Au EDS maps. Scale bar: 5 nm.

shell.²² Our results also have some connection to molecular dynamics simulations of pure and surfactant coated Au NWs that was done by Stefan E. Huber and co-workers. 11 Although the protective coating is quite different from ours, the Huber's simulation results indicated that melting process of pure Au NWs was initiated at the two ends (low coordinated sites) of NWs where atoms exhibited great mobility. The surfactant coating attractive interactions with Au atoms stabilized the coated NWs at high temperatures. In our case, the enhanced thermal stability of Au-Al₂O₃ NWs can be also attributed to the SMSB between Au and Al₂O₃, which successfully suppressed the large-amplitude thermal motions of the gold atoms at low coordinated sites.

Additional X-ray photoelectron spectroscopy (XPS) characterization revealed the chemical states evolution during heating. More specifically, in situ XPS was employed to study Au-Al2O3 core-shell and pure Au NWs before and after vacuum heating at 500 °C. In these experiments, the sample was heated

Communication ChemComm

to 500 °C in the high vacuum XPS chamber for 15 and 30 minutes and cooled down to RT, which was followed by XPS characterization. As shown in Fig. S3a (ESI†), after annealing at 500 °C for 30 minutes, the Au 4f doublets shifted toward lower binding energy (B.E.) from 84.05 eV and 87.80 eV (blue dash line) to 83.85 eV and 87.60 eV (red dash line), respectively. These changes coincided with shrinkage of Au NWs to NPs observed by STEM (Fig. 3). When diameter of Au NWs was small, the hole state caused by photoionization could not be effectively screened by the cores of neighbouring atoms or the conduction electrons, resulting in higher B.E. of Au 4f.²³ After shrinking to NPs, coordination number of Au atoms had increased, resulting in a shift to lower B.E. This observation is consistent with the two spin-orbit split peaks (4f_{5/2} at 88.5 eV and 4f_{7/2} at 84.85 eV) decreasing in intensity during the annealing. More specifically, the intensity of the nano Au $4f_{7/2}$ peaks (blue) decreased significantly as compared to the bulk Au $f_{7/2}$ peaks (green), while the bulk Au $4f_{7/2}$ attributed peaks became dominant with extended heating. In addition to the peaks mentioned above, the satellites of Au 4f doublets were observed in the B.E. range of Al component, where the chemical shifts in B.E. were observed as well (Fig. S3b, ESI†). These satellites were caused by the nonmonochromatic source for X-ray irradiation at higher photon energies. 24 More specifically, Al source was employed in our XPS experiments, as a result, satellites were observed at lower B.E. of 9.8 eV and 11.8 eV for $K\alpha_3$ and $K\alpha_4$ radiation, in addition to the $K\alpha_{1,2}$ radiation which is the only X-ray component from monochromatic source. For example, the $K\alpha_3$ satellites of Au $4f_{7/2}$ and Au $4f_{5/2}$ peaks shifted from 74.2 eV and 77.9 eV to 74.0 eV and 77.7 eV after heating. In contrast, the intensity of Al₂O₃ 2p peaks (74.7 eV) remained almost unchanged during the heating. Overall, the XPS result suggests that the chemical state of Au NWs changed significantly whereas Al states remained the same during the annealing. Combined with TEM and STEM observations, it can be suggested that Au-Al₂O₃ NWs exhibited an improved thermal stability due to SMSB between Au and Al₂O₃.

In summary, the thermal behaviour and elemental distribution of Au-Al₂O₃ core-shell nanowires were investigated by combination of in situ TEM/STEM and XPS characterization during the samples' annealing at 500 °C. SMSB between gold and alumina was manifested in improved thermal stability of Au-Al₂O₃ NWs. The presence of the SMSB can be explained by the attractive interactions between gold and alumina that successfully suppressed large-amplitude thermal motions of the gold atoms, thereby resulting in more stable Au NWs. EDS maps confirmed that the Au-Al₂O₃ NWs remained cylindrical, while pure Au NWs shrank to nanoparticles. Furthermore, XPS showed that Au chemical states changed from those with low coordination numbers to the bulk states, whereas Al species remained unchanged during the heating. The existence of SMSB in Au-Al₂O₃ system provides both an explanation of

the enhanced thermal resistance in Au/Al₂O₃ catalysts and guidance to design of more stable catalysts.

This research used resources of the Center for Functional Nanomaterials (CFN), which is a U.S. Department of Energy Office of Science User Facility, at Brookhaven National Laboratory under Contract No. DE-SC0012704. Financial support from the NSF CBET Award (#2015275) is also acknowledged.

Conflicts of interest

There are no conflicts to declare.

Notes and references

- 1 Q. Wu, C. J. Ridge, S. Zhao, D. Zakharov, J. Cen, X. Tong, E. Connors, D. Su, E. A. Stach, C. M. Lindsay and A. Orlov, J. Phys. Chem. Lett., 2016, 7, 2910-2914,
- 2 C. Qi, S. Zhu, H. Su, H. Lin and R. Guan, Appl. Catal., B, 2013 **138-139**, 104-112.
- 3 C. M. Wang, K. N. Fan and Z. P. Liu, J. Am. Chem. Soc., 2007, 129, 2642-2647.
- 4 D. W. Goodman, Catal. Lett., 2005, 99, 1-4.
- 5 W. Yang, J. Li, X. Cui, C. Yang, Y. Liu, X. Zeng, Z. Zhang and Q. Zhang, Chin. Chem. Lett., 2021, 32, 2489-2494.
- 6 S. Ghosh, S. S. Acharyya, R. Tiwari, B. Sarkar, R. K. Singha, C. Pendem, T. Sasaki and R. Bal, ACS Catal., 2014, 4, 2169–2174.
- 7 C. W. Han, T. Choksi, C. Milligan, P. Majumdar, M. Manto, Y. R. Cui, X. H. Sang, R. R. Unocic, D. Zemlyanov, C. Wang, F. H. Ribeiro, J. Greeley and V. Ortalan, Nano Lett., 2017, 17, 4576-4582.
- 8 N. Ta, J. Liu, S. Chenna, P. A. Crozier, Y. Li, A. Chen and W. Shen, J. Am. Chem. Soc., 2012, 134, 20585–20588.
- 9 J. Wang, A. H. Lu, M. R. Li, W. P. Zhang, Y. S. Chen, D. X. Tian and W. C. Li, ACS Nano, 2013, 7, 4902-4910.
- 10 S. Ivanova, C. Petit and V. Pitchon, Gold Bull., 2006, 39, 3-8.
- 11 S. E. Huber, C. Warakulwit, J. Limtrakul, T. Tsukuda and M. Probst, Nanoscale, 2012, 4, 585-590.
- 12 A. Scheidemann, J. P. Toennies and J. A. Northby, Phys. Rev. Lett., 1990, 64, 1899-1902,
- 13 G. Haberfehlner, P. Thaler, D. Knez, A. Volk, F. Hofer, W. E. Ernst and G. Kothleitner, Nat. Commun., 2015, 6, 8779.
- 14 A. Boatwright, C. Feng, D. Spence, E. Latimer, C. Binns, A. M. Ellis and S. Yang, Faraday Discuss., 2013, 162, 113-124.
- 15 L. F. Gomez, E. Loginov and A. F. Vilesov, Phys. Rev. Lett., 2012, **108**, 155302.
- 16 G. P. Bewley, D. P. Lathrop and K. R. Sreenivasan, Nature, 2006, 441, 588.
- 17 R. J. Donnelly, Annu. Rev. Fluid Mech., 1993, 25, 325-371.
- 18 W. Lueangchaichaweng, N. R. Brooks, S. Fiorilli, E. Gobechiya, K. Lin, L. Li, S. Parres-Esclapez, E. Javon, S. Bals, G. Van Tendeloo, J. A. Martens, C. E. A. Kirschhock, P. A. Jacobs and P. P. Pescarmona, Angew. Chem., Int. Ed., 2014, 53, 1585-1589.
- 19 H. L. Peng, T. Voigtmann, G. Kolland, H. Kobatake and J. Brillo, Phys. Rev. B: Condens. Matter Mater. Phys., 2015, 92, 184201.
- 20 M. A. Shebzukhova, Z. A. Shebzukhov and A. A. Shebzukhov, Bull. Russ. Acad. Sci.: Phys., 2010, 74, 697-704.
- 21 S. Xu, P. Li and Y. Lu, Nano Res., 2018, 11, 625-632.
- 22 V. Sudheeshkumar, A. Lushington, X. Sun and R. W. J. Scott, ACS Appl. Nano Mater., 2018, 1, 6904-6911.
- 23 M. G. Mason, Phys. Rev. B: Condens. Matter Mater. Phys., 1983, 27,
- 24 J. F. Moulder and J. Chastain, Handbook of X-ray Photoelectron Spectroscopy: A Reference Book of Standard Spectra for Identification and Interpretation of XPS Data, Physical Electronics Division, PerkinElmer Corporation, 1992.